

First In Vivo Use of a Capacitive Micromachined Ultrasound Transducer Array–Based Imaging and Ablation Catheter

Douglas N. Stephens, MS, Uyen T. Truong, MD, Amin Nikoozadeh, PhD, Ömer Oralkan, PhD, Chi Hyung Seo, PhD, Jonathan Cannata, PhD, Aaron Dentinger, PhD, Kai Thomenius, PhD, Alan de la Rama, Tho Nguyen, Feng Lin, PhD, Pierre Khuri-Yakub, PhD, Aman Mahajan, MD, PhD, Kalyanam Shivkumar, MD, PhD, Matt O'Donnell, PhD, David J. Sahn, MD

Received April 13, 2011, from the University of California, Davis, California USA (D.N.S.); Oregon Health and Science University, Portland, Oregon USA (U.T.T., D.J.S.); Stanford University, Palo Alto, California USA (A.N., Ö.O., P.K.-Y.); University of Washington, Seattle, Washington USA (C.H.S., M.O.); University of Southern California, Los Angeles, California USA (J.C.); General Electric Global Research, Niskayuna, New York USA (A.D., K.T., F.L.); St Jude Medical Center for Innovation and Strategic Collaboration, Irvine, California USA (A.d.l.R., T.N.); and University of California, Los Angeles, California USA (A.M., K.S.). Revision requested May 18, 2011. Revised manuscript accepted for publication August 15, 2011.

We thank the following individuals for their support and input in our ongoing endeavor: Ken Nguyen, Thaddeus Chodakauskas, PhD, Jennifer Ma, and Judy Schultheis. Kai Thomenius, Aaron Dentinger, and Feng Lin are employed by GE Corporate Research; Alan de la Rama and Tho Nguyen work for St Jude Medical; they are all authors on this article in their capacity as partners in National Institutes of Health Bioengineering Research Partnership grant HL067647, "High-Frequency Ultrasound Array for Intracardiac Imaging" for which David J. Sahn is principal investigator. Douglas N. Stephens and Uyen T. Truong contributed equally to this work.

Address correspondence to David J. Sahn, MD, Department of Pediatric Cardiology, Oregon Health and Science University, 3181 SW Sam Jackson Park Rd, L608, Portland, OR 97239-3098 USA.

E-mail: sahd@ohsu.edu

Abbreviations

CMUT, capacitive micromachined ultrasound transducer; EAM, electroanatomic mapping; ECG, electrocardiographic; ICE, intracardiac echocardiography; ML, microlinear; PZT, lead zirconate titanate; RF, radiofrequency; RFA, radiofrequency ablation; TSI, thermal strain imaging; 3D, 3-dimensional; 2D, 2-dimensional; UCRA, ultrasound-compatible radiofrequency ablation

Objectives—The primary objective was to test in vivo for the first time the general operation of a new multifunctional intracardiac echocardiography (ICE) catheter constructed with a microlinear capacitive micromachined ultrasound transducer (ML-CMUT) imaging array. Secondly, we examined the compatibility of this catheter with electroanatomic mapping (EAM) guidance and also as a radiofrequency ablation (RFA) catheter. Preliminary thermal strain imaging (TSI)-derived temperature data were obtained from within the endocardium simultaneously during RFA to show the feasibility of direct ablation guidance procedures.

Methods—The new 9F forward-looking ICE catheter was constructed with 3 complementary technologies: a CMUT imaging array with a custom electronic array buffer, catheter surface electrodes for EAM guidance, and a special ablation tip, that permits simultaneous TSI and RFA. In vivo imaging studies of 5 anesthetized porcine models with 5 CMUT catheters were performed.

Results—The ML-CMUT ICE catheter provided high-resolution real-time wideband 2-dimensional (2D) images at greater than 8 MHz and is capable of both RFA and EAM guidance. Although the 24-element array aperture dimension is only 1.5 mm, the imaging depth of penetration is greater than 30 mm. The specially designed ultrasound-compatible metalized plastic tip allowed simultaneous imaging during ablation and direct acquisition of TSI data for tissue ablation temperatures. Postprocessing analysis showed a first-order correlation between TSI and temperature, permitting early development temperature-time relationships at specific myocardial ablation sites.

Conclusions—Multifunctional forward-looking ML-CMUT ICE catheters, with simultaneous intracardiac guidance, ultrasound imaging, and RFA, may offer a new means to improve interventional ablation procedures.

Key Words—ablation; capacitive micromachined ultrasound transducer; electroanatomic mapping; electrophysiology; intracardiac echocardiography; intracardiac imaging; microelectromechanical system; thermal strain

Electrophysiologic interventions have had increasing popularity as treatment options for arrhythmias, particularly atrial fibrillation.¹ Atrial fibrillation is the most common arrhythmia, with an incidence of 2 to 3 per 1000 people aged 55 to 64 years annually,² and is associated with considerable morbidity and mortality.^{3,4} There are at least 3 techniques available to interventionalists that can accurately locate intracardiac regions of interest, with

fluoroscopy being the most established technique. However, the exposure to ionizing radiation, as well as the inability of fluoroscopy to clearly delineate subsurface intracardiac regions and confirm catheter contact with the endocardium, has made echocardiography and electroanatomic mapping (EAM) the most attractive as adjunct modalities.^{5–9} Intracardiac echocardiography (ICE), in particular, has found multiple uses in the electrophysiology laboratory, providing real-time display of intracardiac structures.^{6–8}

The use of ultrasound image guidance for interventional radiofrequency ablation (RFA) procedures in the heart has begun to play a more important role in the minimization of fluoroscopic radiation exposure to the patient while imaging important intracardiac features, eg, the membranous fossa of the interatrial septum for puncture access to the left atrium, the pulmonary veins, and Doppler blood velocities associated with pulmonary vein stenosis.¹⁰ Important considerations in the design of ICE catheters are the (1) imaging and handling performance features, (2), compatibility with current interventional practice, and (3) cost in both procedural time and purchasing expense. Overall, a catheter that can be itself guided into place with EAM, perform high-quality image guidance of RFA therapy, and improve procedural throughput at a lower cost is a worthwhile goal. As a general guide, Table 1 compares the common RFA catheter with an “ideal” catheter and with the initial features of a proposed progenitor, a microlinear capacitive micromachined ultrasound transducer (ML-CMUT) catheter.

The miniaturization of ICE catheters has revolutionized interventional procedures by integrating ultrasound transducers onto flexible, low-profile catheters, which allow imaging in the restricted spaces of vascular and cardiac structures.^{11–13} Two distinctly different ICE catheter prototypes, descriptively referred as ML catheters because of their small ultrasonic array designs, have been developed within a program to build a series of miniaturized high-frequency forward-looking transducer arrays.¹⁴ Piezoceramic arrays,

namely those made with lead zirconate titanate (PZT), are considered standard design types for most ultrasound applications. Currently in their third generation of development, our early ML devices are called ML-PZT array catheters. The second array transducer type is the CMUT, now in its second generation of development¹⁵; these CMUT arrays are used in the assembly of the ML-CMUT array catheter (Figure 1). By comparison to PZT, the CMUT as an acoustic transducer is relatively new as an ultrasound transceiver. This silicon-based array, however, has several design aspects that may yield a considerable advantage over the PZT array type, especially at small sizes. The small-element CMUT array in combination with a local buffer-preamplifier offers excellent transmit and receive sensitivity with a wide bandwidth, allows special element shaping, does not require acoustic matching layers, and may be considerably less expensive in large-scale manufacturing.

The principal objective of this work is to describe the first in vivo use of a forward-looking ML-CMUT array catheter in a true 9F profile, the catheter compatibility with EAM guidance, and the use of a specially integrated RFA tip capable of both monitoring and delivery of intracardiac ablation. This work represents the first in vivo ablation and direct simultaneous collection of tissue echo data for the thermal strain temperature at the exact ablation site. In addition, we describe the initial use of the ML-CMUT catheter in exploratory cardiac imaging from the perspective of the epicardial surface from within the pericardium.

Materials and Methods

Microlinear Array Catheters: Differentiation by Array Technology

Although the primary focus of this work is the description and first use of the ML-CMUT catheter equipped with a microelectromechanical system silicon-based array, both

Table 1. Performance Parameter Objectives for Catheters Used in Radiofrequency Ablation Procedures

Catheter Performance Parameter	Ideal Catheter	Standard RFA Catheter	ML-CMUT ICE Catheter
Catheter size, F	6	7	9
Steering bend radius, cm	1	3	3
Electroanatomic mapping guidance capability	Yes	Optional	Yes
RFA capability	Yes	Yes	Yes
RFA electrode bands	Yes	Yes	No
RFA tip electrode	Yes	Optional	Yes
RFA ultrasound image guidance	Yes	No	Yes
Tissue RFA temperature as means of direct guidance	Yes	No	Yes

ICE indicates intracardiac echocardiographic; ML-CMUT, microlinear capacitive micromachined ultrasound transducer; and RFA, radiofrequency ablation.

the PZT and CMUT array technologies and their contributions are briefly reviewed in the following sections for the purpose of general comparison. As a precursor design, the ML-PZT catheter was built with a piezoceramic array¹⁴ with relatively standard building materials; otherwise, the general catheter design and construction for the two types of ML catheters are largely the same. Both catheters have RFA ablation tip electrodes and at least one electrode for EAM compatibility. The ML-PZT catheter has a tip-mounted thermocouple for temperature feedback during ablation procedures. Both types of ML catheters are forward-looking ICE devices with bidirectional steering, which permits image plane elevation up/down positioning. The array of the ML catheters is rectangular and end facing, which allows it the capability to project a B-mode plane directly out from the tip of the catheter.¹⁵ Both array types are constructed with 24 elements with a similar aperture area. The ML-CMUT catheter features described in Table 1 have also been incorporated in the ML-PZT catheter.

The two arrays were designed with slightly different objectives but are compared here for historical context. A more thorough and quantitative design comparison study is planned in the near future.

Microlinear PZT

The early ML catheters used in our research partnership have been constructed of the industry standard ceramic piezoelectric transducer material called PZT. The ML-PZT catheter does not require a special interface circuit near the array but does require fine-line mechanical assembly of the array elements, an acoustic matching layer, and a backing absorber and lacks some of the benefits of CMUT array technology.¹⁶

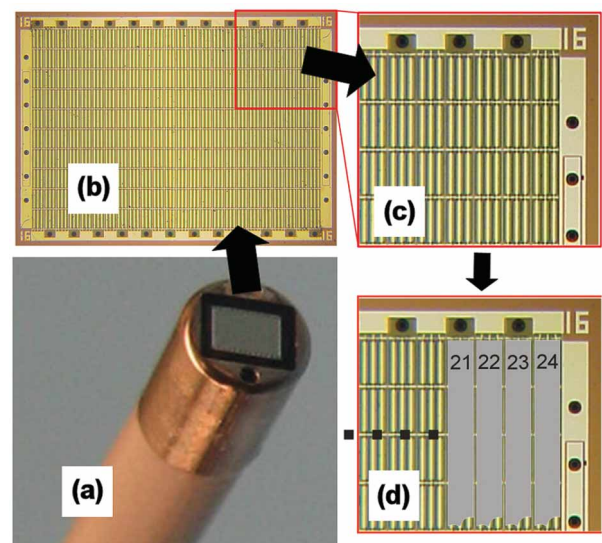
The PZT array transducer in our design uses the flex circuit polyimide itself, together with a single thin encapsulation layer, as the effective acoustic-matching layer for efficient acoustic transmission and reception. The 24-element PZT array aperture is 1.2×1.58 mm, with a center frequency of 14 MHz. The PZT array has an acceptable 50% fractional bandwidth.¹⁴

Microlinear CMUT

The CMUT array design is a competitive option for intracardiac ultrasound transducers offering several performance and manufacturing advantages. Unlike a piezoelectric transducer, which typically vibrates in its thickness direction to generate ultrasound, a CMUT consists of many capacitors with movable top plates connected electrically in parallel and generates ultrasound as a result of these plate vibrations in response to an electrostatic actuation.

Material properties and the thickness of a piezoelectric (eg, PZT) crystal dictate its frequency of operation. Piezoelectric materials most commonly used in transducers for medical imaging are soft piezoelectrics such as PZT-5A and PZT-5H and have an acoustic impedance in the 30- to 36-megarayl range, which is relatively large compared to that of the human body (1.5 megarayls). As a result, a backing and a front-side matching layer are often needed to achieve a wideband response that leads to a short pulse duration for improved axial resolution. On the other hand, the CMUT's ultrasound-producing thin plates have a smaller acoustic impedance than water¹⁷ over a wide frequency range and hence are inherently wideband when operated in immersion or in contact with tissue. The frequency of operation for a CMUT is set primarily by the geometry of its basic building block, the capacitor, and mechanical properties of the plate material, typically silicon or silicon nitride. Capacitive micromachined ultrasound transducer arrays are made with silicon micromachining, which allows more flexibility in the transducer's size, shape, and spacing between elements.¹⁸ In addition, CMUTs have a smaller internal loss and a higher thermal conductivity than PZT transducers, the combination of which results in a reduced tendency to generate and retain heat.¹⁹

Figure 1. Prefinished distal tip (a) of the 9F microlinear capacitive micromachined ultrasound transducer (CMUT) intracardiac imaging catheter with a metal radiofrequency ablation tip electrode, and the 24-element CMUT array (b) with silicon die dimensions of 1.9×1.4 mm. The integrated front-end electronics are bonded underneath the array. The CMUT subelement membranes are shown in c, which constitute the functional element widths depicted in d.



The 24-element CMUT array aperture is 1.073×1.50 mm, with a center frequency of 8.5 MHz. The CMUT array has a 74% fractional bandwidth, with an absolute frequency bandwidth which is quite close to that of the PZT array design. Optimization of the frequency band of operation is an important design consideration; future work will provide guidance on this aspect. In addition to the unique CMUT array design, the array is buffered electronically with a flip-chip bonded application-specific integrated circuit,^{16,20} which permits direct transmit pulse control from the system and also offers a transimpedance amplifier to enhance the receive echo fidelity. The amplifier provides a local signal boost, which is needed to adequately drive the low electrical impedance coax used in the catheter.

Real-time Navigational Methods

Fluoroscopy is recognized as the standard for interventional catheter guidance, even with its incumbent ionizing radiation hazard to the patient, limited view of catheters, and inability to show 3-dimensional (3D) views. In most studies performed, we exploited the benefits of EAM in addition to fluoroscopic guidance. Electroanatomic mapping can offer a real-time 3D view for anatomic localization within the heart. It has been developed over the last decade in several different formats^{21–23} and has the real potential for virtually replacing much of fluoroscopy,^{8,24–29} which is especially valuable in pediatric cases. Electroanatomic mapping procedures require some time to first map the chamber of interest. Once that is accomplished, real-time tracking of other catheters can be easily performed, which provides positional feedback. Positional records of ablation events with markers on the EAM endocardial wall display were used in most of our studies. Before the vascular introduction of the ML catheters, a separate 7F mapping catheter was used with the Ensite NavX navigation and visualization technology system (St Jude Medical, Inc, St Paul, MN) to obtain the 3D real-time endocardial geometry of the right atrial and right ventricular chambers.

Thermal Strain Imaging

The current methods of RFA procedural feedback are limited principally to monitoring the radiofrequency (RF) power, electrode contact, and catheter tip temperature (which correlate relatively poorly with the actual subsurface tissue temperature, especially in irrigated tip catheters). Intracardiac echocardiographic image guidance can monitor undesirable bubble formation³⁰ during RFA, but it has obvious drawbacks in the procedural time and multiple catheter handling. Recent efforts have shown that even optical monitoring of cardiac tissue during RFA may yield

feedback information.³¹ Direct tissue temperature monitoring with a minimally invasive approach is likely one of the better methods to pursue. A means of extracting the treated tissue temperature information has been developed using the apparent “thermal strain” (ie, change in ultrasound speed with temperature) detected ultrasonically during the RFA process itself.

Thermal strain imaging (TSI), derived from phase-sensitive speckle tracking of ultrasound images, which has been well described as a novel tissue differentiation technique,^{32,33} can also be used to create images based on the temperature dependence of the sound speed. Thermal strain imaging has already been successfully used in atherosclerosis detection and tissue characterization.^{33–37}

Direct observation of the dynamic temperature changes occurring in subendocardial surface tissue (not just surface temperature) concurrent in the time course of ablation has long been a goal for better RFA procedural feedback. A special ultrasound-compatible radiofrequency ablation (UCRA) tip has been made to fit over the distal tip of the ML catheters to enable this ability (Figure 2). The tip is made primarily of a plastic (TPX, Polymethylpentene; Mitsui Chemicals, Inc, Tokyo, Japan) with a very thin ($\approx 3\text{-}\mu\text{m}$) metallization layer coating the outside surface. This tip metal is electrically connected to the RFA tip of the ML catheter, which permits the thin metallization to act as the RFA electrode itself. The UCRA tip is equipped with holes that allow blood to exist (or saline irrigation fluid) within the tip so the ML array ultrasonic wave energy may traverse this liquid path and through the tip wall. Ultrasound imaging of the actual ablation tissue during the process of RFA is then possible. In an attempt to reduce RFA electronic noise interference during active ablation, the electrocardiographic (ECG) signal was also used to gate the ablation during systole, whereas echo data frames were taken during diastole for TSI temperature processing.

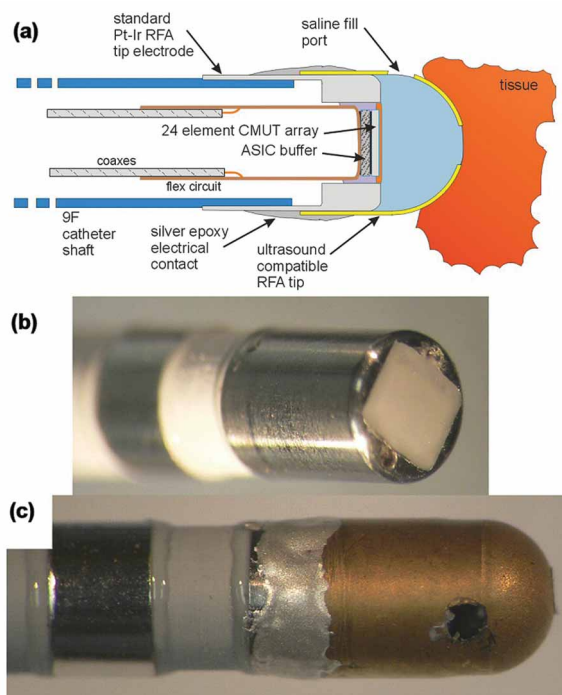
To process echo data for TSI (in an offline fashion, which was preferred given the early stage of development of the specific technique), 4 frames of data with the least motion were selected by examining B-mode images from the first cardiac cycle before ablation. Using these as reference frames, 2D cross-correlation was performed to find the best matched frame with the highest cross-correlation (≥ 0.85) within a cycle for all subsequent cardiac phases. Then, using each frame from the first cardiac cycle as a reference, 2D speckle tracking was performed with all corresponding frames throughout the experiment. These 4 displacement sets were averaged to produce the measured axial displacement. Two-dimensional phase-sensitive correlation-based speckle tracking³⁸ was applied to the RF

data from every frame in the sequence to estimate temporal strain along the axial direction.

Animal Studies

Animal model studies were performed with approval by the Institutional Animal Care and Use Committees of both institutional sites, University of California, Los Angeles, and Oregon Health and Science University. The study protocol was developed by the Bioengineering Research Partnership “High-Frequency Ultrasound Arrays for Cardiac Imaging,” which has successfully produced a family of ICE catheters and various technologies³⁹ for use in electrophysiology. The ML ICE catheters were tested in 5 porcine models (35–45 kg) under general anesthesia with 2% isoflurane and mechanical ventilation. The ECG and oxygen saturation were monitored continuously throughout the study. Access for various experimental protocols was obtained via femoral veins and arteries as well as jugular veins.

Figure 2. Graphic depiction (a) of a microlinear capacitive micromachined ultrasound transducer (CMUT) catheter with the special ultrasound transparent ablation tip, which contacts the endocardial wall for radiofrequency ablation (RFA) and simultaneous thermal strain echo collection. The tip thermocouple and steering assembly are omitted for clarity. Actual images show the catheter without the special tip (b) and after the tip attachment procedure (c). ASIC indicates application-specific integrated circuit; and Pt-Ir, platinum-iridium.



Fluoroscopy was used in all cases to advance catheters from access vessel sites. Electroanatomic mapping⁴⁰ was subsequently used to delineate the 3D endocardial borders of the right atrium and right ventricle and serve as both a means of guidance and record of ablation site locations. Radiofrequency ablation procedures with either a standard RFA catheter (Livewire catheter, 4-mm tip; St Jude Medical, Inc) or with an ML catheter equipped with the UCRA tip were performed with a conventional Stockert generator (Biosense-Webster, Diamond Bar, CA) or a modified IBI generator (St Jude Medical, Inc) equipped with customized ECG-gated RFA capability. Images from the CMUT catheter were obtained alternatively with both the Vivid 7 and Vivid *i* imaging systems (GE Healthcare, Milwaukee, WI).

Imaging characteristic and thermal strain analyses were accomplished using both types of ML catheters with 2D phased array sector displays and the tissue Doppler strain imaging mode operated on the Vivid 7 imaging system at a transducer frequency of 12 MHz. Both high-frame rate (120 frames per second) gray scale images and low-frame rate (4 frames per second) thermal strain baseband I (complex, real part) and Q (complex, imaginary part) data frames were obtained and processed offline on an EchoPAC Clinical Workstation (GE Healthcare, Wauwatosa, WI) and MATLAB software (The MathWorks, Natick, MA), respectively.

Results

In Vivo Studies: Qualitative Comparisons to the ML-PZT Catheter

The ML-PZT catheter was typically used first to establish an operational baseline for comparison to the ML-CMUT catheter. Catheter introduction was accomplished through either jugular or femoral venous access and was positioned inside the lateral right atrium pointing forward toward the epicardial surface.

The first generation of ML-PZT catheters had 9F catheter shafts and rather large 15F tip enclosures.⁴¹ With a similar early history, the current second-generation ML-CMUT prototype catheter is now much smaller than the first-generation catheter with improved steerability, although we encountered catheter shaft kinking in 1 of the 5 catheters used, which restricted intracardiac maneuverability.

The ML-CMUT prototype catheters imaged well without substantial technical difficulties and were able to delineate intracardiac structures to a depth reaching 3 cm. The image quality of these first-use in vivo ML-CMUT catheters presented itself favorably in comparison to the more mature ML-PZT catheter design (Figure 3).

To additionally observe the image penetration and catheter handling of the ML-CMUT, an epicardial study was undertaken. In one animal model, the ML-CMUT catheter was introduced percutaneously into the sub-xiphoid region and advanced into the pericardial space under fluoroscopic guidance. The catheter was steered around the lateral and posterior regions of the heart to the right atrium (Figure 4). We found, as did two previous studies using ICE catheters in the intrapericardial space,^{42,43} that intracardiac structures were delineated with excellent image stability, including the left atrial appendage image.

In Vivo Studies: ML-CMUT Catheter Guidance

The ML-CMUT catheter was used to guide the position of a separate RFA catheter as well as operate with the NavX EAM system to permit tracking of the ML-CMUT catheter tip’s 3D position. Figure 5 shows an ML-CMUT catheter guiding a separate RFA catheter near the inferior right atrial isthmus. The ML-CMUT catheter position could also be tracked easily in an EAM-mapped heart chamber (Figure 6). A single-ring electrode very near the catheter tip was used as the active EAM electrode; the catheter tip could be tracked in any position within the porcine heart right atrial and right ventricular chambers. The NavX EAM system was used as in previous

Figure 3. Qualitative image quality comparison of the microelectromechanical system–based second-generation microlinear capacitive micromachined ultrasound transducer (ML-CMUT) prototype (left) and the third-generation piezoceramic microlinear lead zirconate titanate transducer (right), with system image sizes adjusted to correct for scale. Both were used in these examples to help guide the ablation tip of a separate radiofrequency ablation (RFA) catheter into position on the surface of the endocardium. The ML-CMUT image (left) shows the RFA catheter surrounded by a collection of echogenic bubbles near the tip (arrows) during an ablation procedure.

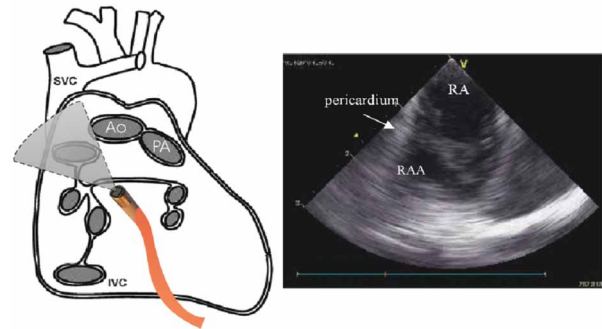
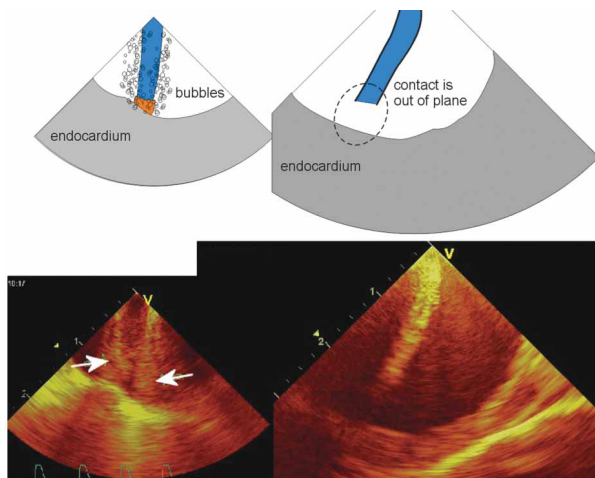


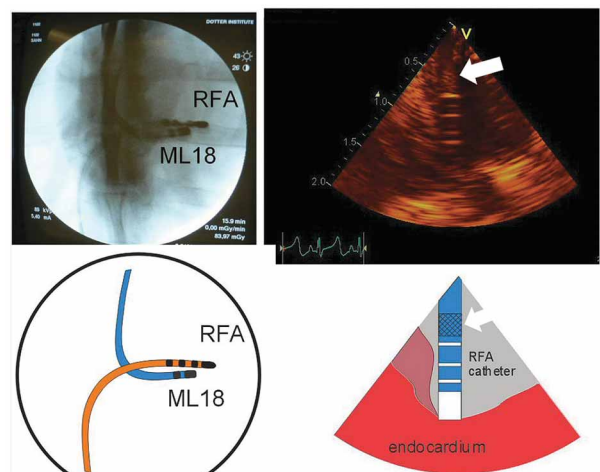
Figure 4. Imaging the right atrium (RA) and appendage from the oblique sinus within the pericardial sac while investigating catheter steering and the potential for an epicardial ultrasound examination with the microlinear capacitive micromachined ultrasound transducer catheter. Ao indicates aorta; IVC, inferior vena cava; PA, pulmonary artery; RAA, right atrial appendage; and SVC, superior vena cava.

studies^{14,44} to maintain a spatial map of the ablation sites visited. After the specific site ablation studies, the porcine heart was explanted and examined (Figure 7).

In Vivo Studies: Feasibility of TSI With the ML-CMUT

The ML-CMUT catheter was used with the specially developed UCRA tip to compare its general TSI capability to that of the ML-PZT version of the catheter. Details of ML-PZT use with this tip are reported in related works.^{45,46}

Figure 5. Microlinear capacitive micromachined ultrasound transducer (ML-CMUT; ML 18) catheter imaging the placement of a radiofrequency ablation (RFA) catheter near the inferior right atrial isthmus. The imaging catheter has been advanced from the superior vena cava, whereas the RFA catheter was introduced femorally. The wide-bandwidth ML-CMUT here can resolve the very fine wire braid pattern (arrow) within the RFA catheter shaft in the range (at ≈5 mm) of the best focus for this small tip-mounted array.



The ML-CMUT prototype, assembled using the UCRA tip, was preloaded with saline to avoid air bubbles in the acoustic imaging path (Figure 2). Using a modified RF generator (IBI 1500-T11; St Jude Medical, Inc) to permit ECG trigger-controlled ablation pulses, the typical ablation parameters were 30 to 50 W of RF generator power, 70 to 80 Ω of contact resistance, 40 seconds of ablation, and a tip temperature (using the standard-mount thermocouple in the ML RFA electrode) limit set for 65°C. As tested with the ML-PZT catheter, the ML-CMUT catheter could successfully image simultaneously during RFA procedures with only minor artifacts from either RF electrical or acoustic (UCRA tip) sources.

Echo frame data were analyzed for temperature as a function of ablation time. In the echo frame analysis, it was assumed for simplicity that the cardiac tissue returns to its original physical position at end systole while observed in a state without ablation. Electrocardiographically triggered ablation in some cases was not possible during image acquisition because of a weak ECG signal that was overwhelmed by RFA signal interference.

For comparison purposes, Figure 8 shows in vivo-derived thermal strain data from both the ML-PZT and the ML-CMUT catheters. Both catheters were built with the special UCRA tip (Figure 2); however, only the ML-PZT catheter had a thermocouple embedded directly into the UCRA tip for direct endocardial surface temperature recording.

Figure 6. The microlinear capacitive micromachined ultrasound transducer (ML-CMUT) ablation sites recorded in the porcine model are indicated as numbered red dots. The NavX reconstruction of the partially mapped right heart is shown in two anterior views. The electroanatomic mapping catheter was advanced from the inferior vena cava (IVC) and used to define the right atrial (RA) and right ventricular (RV) chambers before tracking ML-CMUT ablation locations. Ablations were performed to test the handling of the ML-CMUT in the RA, through the tricuspid annulus (TA) to the RV, and additionally in the coronary sinus (CS) and great cardiac vein.

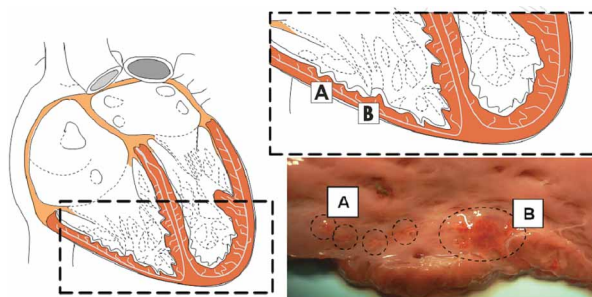
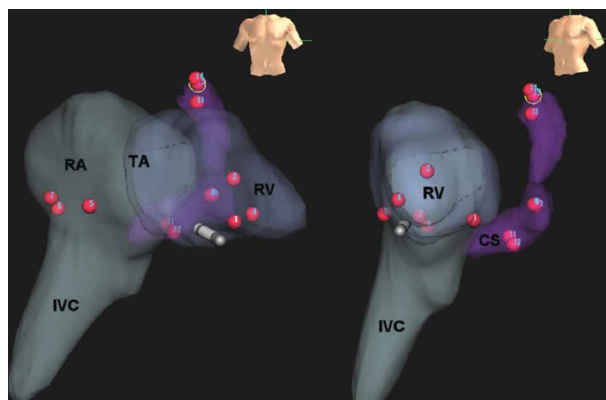
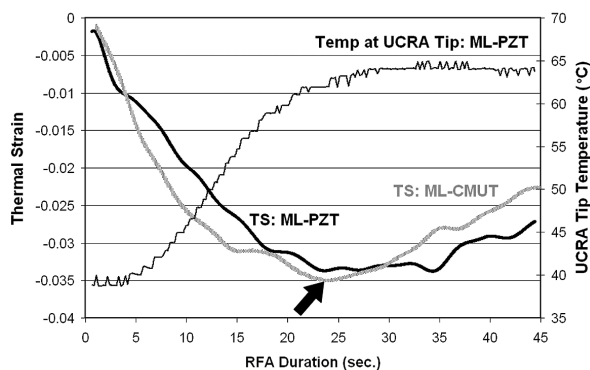


Figure 7. The microlinear capacitive micromachined ultrasound transducer ablation sites (A indicates region of single ablations; and B, multiple ablations) located in the porcine right ventricular free wall are shown explanted subsequent to radiofrequency ablation. These sites showing erythematous endocardium corresponded well to the NavX electroanatomic mapping–recorded ablation site record.

perature recording. The ultrasound-derived thermal strain data are computed from a tissue site deeper (2–5 mm) and thus will be a different temperature than the endocardial surface, probably slightly cooler. Further experiments to examine the actual in vivo temperature distribution as produced from RFA are planned. As expected, heart motion artifacts can be minimized with ECG triggering and special signal processing as described earlier. Mechanical ventilation was stopped during image collection to reduce tissue motion artifacts. Figure 9 shows B-

Figure 8. Comparison of the in vivo time course of ultrasound-based thermal strain (TS) between the microlinear lead zirconate titanate (ML-PZT) and microlinear capacitive micromachined ultrasound transducer (ML-CMUT) catheters for ablations under identical conditions performed on the right ventricular endocardial wall. The arrow shows the strong non-linear TS response, which becomes more pronounced as the tissue heating continues. Further in vivo characterization of this response is an important focus of future studies. RFA indicates radiofrequency ablation; and UCRA, ultrasound-compatible radiofrequency ablation.



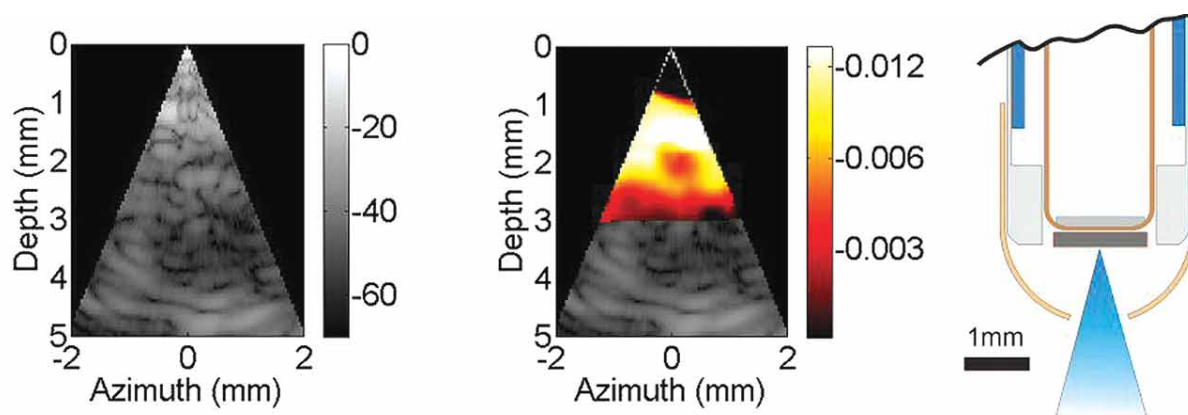


Figure 9. Thermal strain imaging based on in vivo echoes from a porcine endocardium undergoing simultaneous ablation. The far left panel is the unprocessed B-mode sector image in gray scale gradients on a decibel scale. The middle panel shows the ultrasound-based “strain” image of the tissue approximately 12 seconds after the start of ablation; the round dark region at a 2-mm depth is likely a small blood vessel. The color bar describes the (unitless) thermal strain, which can be converted to temperature units (as suggested in Figure 8) pending verification of the scaling factor relationship, which is to be determined. A schematic of the ultrasound-compatible radiofrequency ablation tip and approximate ultrasound image sector is shown at the far right.

mode images and B-mode images overlaid with TSI 12 seconds after the initiation of ablation, which corresponded to approximately the peak TSI strain magnitude. Thermal strain image-processing techniques are in development to reduce the effects of heart motion and enhance the speed of data processing.

With regard to negative findings during RFA, artifacts resulting from minor RF electrical noise emissions compromised imaging but not excessively. This electrical noise affected the quality of electrocardiographic triggering as well.

Discussion

We previously described an early-generation 9F ML-PZT catheter design, which showed an echo penetration depth of only 2 cm.¹⁴ In consideration of the piezoceramic array aperture dimensions of only 1.2×1.58 mm, the image quality was within expectations and useful for near-field ICE imaging. In more recent experiments, we were able to test the third generation of this ML-PZT prototype with the benefit of improved array assembly, which showed image penetration improvement to a depth of 4 cm. Additionally, steerability in the catheter has improved in every prototype generation produced, although slight kinking limited its motion. This purely mechanical issue can be remedied by optimizing the catheter wall material for strength and shore durometer hardness.

We expect a similar performance development pathway for the ML-CMUT catheter. Once the ML-CMUT design has matured, a more quantifiable comparison study

with the ML-PZT catheter will be attempted. The second-generation ML-CMUT catheter, presented in this work, has shown promise as a competitive alternative to the ML-PZT design, currently with 3 cm of depth penetration. The use of these recently developed CMUT catheters is still in its infancy, with many of the special array features still to be fully exploited. Capacitive micromachined ultrasound transducer and application-specific integrated circuit assembly techniques are improving along with methods to improve the array-buffering circuitry and high-voltage direct current bias generation and isolation. The ML-CMUT echo signal fidelity benefited greatly from the addition of small application-specific integrated circuit direct current supply capacitors (100 nanofarads), which prevent amplifier feedback oscillation.

Beyond the fundamental catheter performance features of the ML-CMUT, its compatibility with EAM intracardiac guidance is essential for this design to reach its full multifunctional potential. We expect specially equipped RFA guidance catheters in the future to be positioned within the heart by nonionizing visualization technologies such as EAM and the implementation of local ablation feedback through the acquisition of actual tissue temperature indications derived from the multifunctional catheter itself.

Decreased reliance on fluoroscopically guided interventions in electrophysiologic studies will become more important in the future,⁴⁷ which is particularly relevant in pediatric patients, for whom ablation procedures may last 40 to 60 minutes.^{48,49} In this particularly vulnerable group, clinicians need to consider the lifetime radiation cumula-

tive risk. Studies have already shown that an improved navigational system used during ablation procedures can substantially decrease the duration of both ablation procedures and fluoroscopic positioning without altering the success or complication rate.^{50,51} Interest now is expanding with regard to the extent that echocardiography can shift the paradigm in imaging guidance during ablation.^{52,53}

Offline processing of the TSI data collected during RFA shows the feasibility of tissue temperature estimation. Work is under way to further assess the temperature estimation accuracy and to integrate TSI processing for real-time displays. Because the relationship between the ultrasound-based thermal strain and actual tissue temperature is approximately linear only to 50°C, the expected clinical use will be to provide the interventionalist with an effective indicator of the sufficiency of a thermal dose to help prevent excessive ablations, which can produce undesirable consequences such as phrenic nerve damage and pulmonary vein stenosis.

In conclusion, the image quality attained by the ML-CMUT catheters, as well as their ability to penetrate 3 cm of tissue, is considerable given the fact that they have a small imaging aperture of less than 1.5 × 2 mm. This second generation of the ML-CMUT catheter has improved steerability, which allows it to be manipulated more easily in the confines of the heart, and has the potential for expanded imaging use in the pericardial space. Microlinear CMUT catheters, in addition to the ML-PZT catheters, have been successfully used to collect potentially meaningful temperature information through the use of thermal strain processing. This promising approach may substantially influence real-time ablation guidance in future clinical practice. Alternative catheter designs, currently in development, aim toward further increasing therapeutic effectiveness by delivering a high-intensity focused ultrasonic beam as the energy source for ablation.

References

1. Wang LX, Xue YZ. Contemporary management of atrial fibrillation: a brief review. *Adv Med Sci* 2010; 55:130–136.
2. Falk RH. Atrial fibrillation. *N Engl J Med* 2001; 344:1067–1078.
3. van Walraven C, Hart RG, Wells GA, et al. A clinical prediction rule to identify patients with atrial fibrillation and a low risk for stroke while taking aspirin. *Arch Intern Med* 2003; 163:936–943.
4. Hart RG, Benavente O, McBride R, Pearce LA. Antithrombotic therapy to prevent stroke in patients with atrial fibrillation: a meta-analysis. *Ann Intern Med* 1999; 131:492–501.
5. Vaina S, Ligthart J, Vijayakumar M, et al. Intracardiac echocardiography during interventional procedures. *EuroIntervention* 2006; 1:454–464.
6. Dello Russo A, Casella M, Pelargonio G, et al. Intracardiac echocardiography in electrophysiology. *Minerva Cardioangiol* 2010; 58:333–342.
7. Reddy VY, Morales G, Ahmed H, et al. Catheter ablation of atrial fibrillation without the use of fluoroscopy. *Heart Rhythm* 2010; 7:1644–1653.
8. Ferguson JD, Helms A, Mangrum JM, et al. Catheter ablation of atrial fibrillation without fluoroscopy using intracardiac echocardiography and electroanatomic mapping. *Circ Arrhythm Electrophysiol* 2009; 2:611–619.
9. den Uijl DW, Blom NA, Wijnmaalen AP, Bax JJ, Schalij MJ, Zeppenfeld K. Real-time integration of intracardiac echocardiography to facilitate atrial tachycardia ablation in a patient with a Senning baffle. *Circ Arrhythm Electrophysiol* 2009; 2:e28–e30.
10. Holmes DR Jr, Monahan KH, Packer D. Pulmonary vein stenosis complicating ablation for atrial fibrillation: clinical spectrum and interventional considerations. *JACC Cardiovasc Interv* 2009; 2:267–276.
11. Valdes-Cruz LM, Sideris E, Sahn DJ, et al. Transvascular intracardiac applications of a miniaturized phased-array ultrasonic endoscope: initial experience with intracardiac imaging in piglets. *Circulation* 1991; 83:1023–1027.
12. Cyran SE, Kimball TR, Meyer RA, et al. Efficacy of intraoperative transesophageal echocardiography in children with congenital heart disease. *Am J Cardiol* 1989; 63:594–598.
13. Packer DL, Stevens CL, Curley MG, et al. Intracardiac phased-array imaging: methods and initial clinical experience with high resolution, under blood visualization—initial experience with intracardiac phased-array ultrasound. *J Am Coll Cardiol* 2002; 39:509–516.
14. Stephens DN, O'Donnell M, Thomenius K, et al. Experimental studies with a 9F forward-looking intracardiac imaging and ablation catheter. *J Ultrasound Med* 2009; 28:207–215.
15. Nikoozadeh A, Wygant IO, Lin DS, et al. Forward-looking intracardiac ultrasound imaging using a 1-D CMUT array integrated with custom front-end electronics. *IEEE Trans Ultrason Ferroelectr Freq Control* 2008; 55:2651–2660.
16. Wygant IO, Jamal NS, Lee HJ, et al. An integrated circuit with transmit beamforming flip-chip bonded to a 2-D CMUT array for 3-D ultrasound imaging. *IEEE Trans Ultrason Ferroelectr Freq Control* 2009; 56:2145–2156.
17. Demirci U, Ergun AS, Oralkan O, Karaman M, Khuri-Yakub BT. Forward-viewing CMUT arrays for medical imaging. *IEEE Trans Ultrason Ferroelectr Freq Control* 2004; 51:887–895.
18. Wong SH, Kupnik M, Watkins RD, Butts-Pauly K, Khuri-Yakub BT. Capacitive micromachined ultrasonic transducers for therapeutic ultrasound applications. *IEEE Trans Biomed Eng* 2009; 57:114–123.
19. Ergun AS, Huang Y, Zhuang X, Oralkan O, Yaralioglu GG, Khuri-Yakub BT. Capacitive micromachined ultrasonic transducers: fabrication technology. *IEEE Trans Ultrason Ferroelectr Freq Control* 2005; 52:2242–2258.
20. Nikoozadeh A, Oralkan O, Gencel M, et al. Forward-looking intracardiac imaging catheters using fully integrated CMUT arrays. Paper presented at: IEEE 2010 International Ultrasonics Symposium; October 11–14, 2010; San Diego, CA.
21. Gepstein L, Hayam G, BenHaim SA. A novel method for nonfluoroscopic catheter-based electroanatomical mapping of the heart: in vitro and in vivo accuracy results. *Circulation* 1997; 95:1611–1622.

22. Wittkamp FHM, Wever EFD, Derksen R, et al. LocaLisa: New technique for real-time 3-dimensional localization of regular intracardiac electrodes. *Circulation* 1999; 99:1312–1317.
23. Earley MJ, Showkathali R, Alzetani M, et al. Radiofrequency ablation of arrhythmias guided by non-fluoroscopic catheter location: a prospective randomized trial. *Eur Heart J* 2006; 27:1223–1229.
24. Shepherd EJ, Gall SA, Furniss SS. Interatrial septal puncture without the use of fluoroscopy: reducing ionizing radiation in left atrial ablation procedures. *J Interv Card Electrophysiol* 2008; 22:183–187.
25. Drago F, Silveti MS, Di Pino A, Grutter G, Bevilacqua M, Leibovich S. Exclusion of fluoroscopy during ablation treatment of right accessory pathway in children. *J Cardiovasc Electrophysiol* 2002; 13:778–782.
26. Grubb N, Petzer E, Lang C, et al. A zero fluoroscopy approach for electrophysiology studies and catheter ablation for common supraventricular tachycardias [abstract]. *Heart* 2006; 92(suppl):A147.
27. Schwartzman D, Zhong H. On the use of CartoSound for left atrial navigation. *J Cardiovasc Electrophysiol* 2010; 21:656–664.
28. Tuzcu V. A nonfluoroscopic approach for electrophysiology and catheter ablation procedures using a three-dimensional navigation system. *Pacing Clin Electrophysiol* 2007; 30:519–525.
29. Smith G, Clark JM. Elimination of fluoroscopy use in a pediatric electrophysiology laboratory utilizing three-dimensional mapping. *Pacing Clin Electrophysiol* 2007; 30:510–518.
30. Alaeddini J, Wood MA, Lee BP, Ellenbogen KA. Incidence, time course, and characteristics of microbubble formation during radiofrequency ablation of pulmonary veins with an 8-mm ablation catheter. *Pacing Clin Electrophysiol* 2006; 29:979–984.
31. Fleming CP, Quan KJ, Wang H, Amit G, Rollins JM. In vitro characterization of cardiac radiofrequency ablation lesions using optical coherence tomography. *Opt Express* 2010; 18:3079–3092.
32. Huang SW, Kim K, Witte RS, Olafsson R, O'Donnell M. Inducing and imaging thermal strain using a single ultrasound linear array. *IEEE Trans Ultrason Ferroelectr Freq Control* 2007; 54:1718–1720.
33. Shi Y, Witte RS, O'Donnell M. Identification of vulnerable atherosclerotic plaque using IVUS-based thermal strain imaging. *IEEE Trans Ultrason Ferroelectr Freq Control* 2005; 52:844–850.
34. Shi Y, Witte RS, Milas SM, et al. Microwave-induced thermal imaging of tissue dielectric properties. *Ultrason Imaging* 2003; 25:109–121.
35. Pereira FR, Machado JC, Foster FS. Ultrasound characterization of coronary artery wall in vitro using temperature-dependent wave speed. *IEEE Trans Ultrason Ferroelectr Freq Control* 2003; 50:1474–1485.
36. Kim K, Huang SW, Hall TL, Witte RS, Chenevert TL, O'Donnell M. Arterial vulnerable plaque characterization using ultrasound-induced thermal strain imaging (TSI). *IEEE Trans Biomed Eng* 2008; 55:171–180.
37. Seip R, VanBaren P, Cain CA, et al. Noninvasive real-time multipoint temperature control for ultrasound phased array treatments. *IEEE Trans Ultrason Ferroelectr Freq Control* 1996; 43:1063–1073.
38. Lubinski MA, Emelianov SY, O'Donnell M. Speckle tracking methods for ultrasonic elasticity imaging using short-time correlation. *IEEE Trans Ultrason Ferroelectr Freq Control* 1999; 46:82–96.
39. Stephens DN, Cannata J, Liu R, et al. Multifunctional catheters combining intracardiac ultrasound imaging and electrophysiology sensing. *IEEE Trans Ultrason Ferroelectr Freq Control* 2008; 55:1570–1581.
40. Ventura R, Rostock T, Klemm HU, et al. Catheter ablation of common-type atrial flutter guided by three-dimensional right atrial geometry reconstruction and catheter tracking using cutaneous patches: a randomized prospective study. *J Cardiovasc Electrophysiol* 2004; 15:1157–1161.
41. Sahn DJ, Stephens DN, Cannata JM, et al. A family of intracardiac ultrasound imaging devices designed for guidance of electrophysiology ablation procedures. *Conf Proc IEEE Eng Med Biol Soc* 2009; 2009:1913–1917.
42. Horowitz BN, Vaseghi M, Mahajan A, et al. Percutaneous intrapericardial echocardiography during catheter ablation: a feasibility study. *Heart Rhythm* 2006; 3:1275–1282.
43. Rodrigues AC, d'Avila A, Houghtaling C, Ruskin JN, Picard M, Reddy VY. Intrapericardial echocardiography: a novel catheter-based approach to cardiac imaging. *J Am Soc Echocardiogr* 2004; 17:269–274.
44. Li XK, Pemberton J, Thomenius K, et al. Development of an electrophysiology (EP)-enabled intracardiac ultrasound catheter integrated with NavX 3-dimensional electrofield mapping for guiding cardiac EP interventions: experimental studies. *J Ultrasound Med* 2007; 26:1565–1574.
45. Stephens DN, Cannata J, Seo CH, et al. Ultrasound-compatible RF ablation electrode design for catheter-based guidance of RF ablation: in vivo results with thermal strain imaging. Paper presented at: IEEE 2010 International Ultrasonics Symposium; October 11–14, 2010; San Diego, CA.
46. Seo CH, Stephens DN, Cannata J, et al. The feasibility of using thermal strain imaging to regulate energy delivery during intracardiac radiofrequency ablation. *IEEE Trans Ultrason Ferroelectr Freq Control* 2011; 58:1406–1417.
47. Rosenthal LS, Mahesh M, Beck TJ, et al. Predictors of fluoroscopy time and estimated radiation exposure during radiofrequency catheter ablation procedures. *Am J Cardiol* 1998; 82:451–458.
48. Geise RA, Peters NE, Dunnigan A, Milstein S. Radiation doses during pediatric radiofrequency catheter ablation procedures. *Pacing Clin Electrophysiol* 1996; 19:1605–1611.
49. Kovoov P, Ricciardello M, Collins L, Uther JB, Ross DL. Risk to patients from radiation associated with radiofrequency ablation for supraventricular tachycardia. *Circulation* 1998; 98:1534–1540.
50. Perisinakis K, Theocharopoulos N, Damilakis J, Manios E, Vardas P, Gourtsoyannis N. Fluoroscopically guided implantation of modern cardiac resynchronization devices: radiation burden to the patient and associated risks. *J Am Coll Cardiol* 2005; 46:2335–2339.
51. Papez AL, Al-Ahdab M, Dick M II, Fischbach PS. Impact of a computer assisted navigation system on radiation exposure during pediatric ablation procedures. *J Interv Card Electrophysiol* 2007; 19:121–127.
52. Stellbrink C, Siebels J, Hebe J, et al. Potential of intracardiac ultrasonography as an adjunct for mapping and ablation. *Am Heart J* 1994; 127:1095–1101.
53. Yin L, Laske TG, Rakow N, et al. Intracardiac echocardiography-guided His bundle pacing and atrioventricular nodal ablation. *Pacing Clin Electrophysiol* 2008; 31:536–542.